5th International Symposium on Three-Dimensional Electromagnetics
Sapporo, Japan, May 7-9, 2013

Tailored fit-for-purpose 3D interpretation of marine CSEM data

Max A. Meju[1]
[1]Petronas Carigali, Kuala Lumpur, Malaysia

SUMMARY

Three-dimensional 3D surveying has now emerged as the method of choice in marine controlled-source electromagnetic (CSEM) exploration for hydrocarbons, but there are limitations in the way that field data are currently interpreted. A major challenge is how to consistently interpret data from 3D surveys to recover the correct physical parameters (specifically, the lateral limits, depth location and electrical resistivity) of potential hydrocarbon-saturated reservoirs in the presence of complex geological overburden. Here, a simple tailored approach is proposed for effective interpretation of CSEM survey data, made possible by 3D edge-detection attributes analysis and accurate background resistivity determination. The determination of the exact background resistivity at each receiver location facilitates the assessment of near-surface heterogeneity and burial-depth of significant resistors, while the use of edge-detection attributes helps constraint the lateral limits of potential 3D resistors, such that a 'fit-for-purpose' iterative inverse modelling approach can be used to improve the constrained estimation of subsurface targets and the assessment of model uncertainty on simple computational platforms. This approach is demonstrated using CSEM survey data from a deepwater fold-and-thrust belt setting.

Keywords: Marine CSEM interpretation, exact background resistivity, 3D edge-detection attributes, tailored inverse modeling, case study

INTRODUCTION

Marine controlled-source electromagnetic (CSEM) methods now find routine applications in oil, gas and hydrates investigations (see e.g., Darnet et al., 2007, Lovatini et al., 2010). Conventional interpretation of CSEM 3D survey data commonly involves the following steps (see e.g. Lovatini et al., 2010): (1) qualitative interpretation of normalised data to determine presence of anomalies and their trends; (2) 1D/2D isotropic or anisotropic inversions to constrain the thicknesses of resistors (possibly using structural details furnished by seismic reflection) and the background resistivity to use for subsequent 3D modelling; (3) 3D forward modelling to validate the adopted background resistivities and any incorporated a priori marker horizons from seismic reflectivity; (4) 3D inversion of inline and broadside CSEM data, and (5) Model appraisal involving validation with seismic sections typified by CSEM image co-rendering or immersion within seismic 3D cubes.

In step (1), data normalisation is commonly done using synthetic background model response or that of a selected off-target receiver site. However, the presence of heterogeneous overburden or seafloor topography could significantly distort the target response (see e.g. Sasaki & Meju, 2009; Sasaki 2010). It could also negate the use of 1D/2D inversion in step 2. It is practically expedient to determine the exact local background resistivities for improved anomaly resolution. Knowing the background resistivity variation in different measurement directions also provides a simple means for assessing the requirement for anisotropy or transverse isotropy in resistivity modelling in steps 2 and 3.

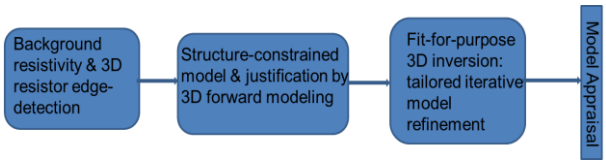

Figure 1. A tailored fit-for-purpose 3D CSEM interpretation workflow.

A simple effective workflow (**Fig 1**) is described herein which permits a consistent and rapid 3D interpretation of CSEM surveys. It effectively addresses the issues embraced in the conventional steps 1 to 5 using data-driven pre-processing and follow-up model-driven processing of 3D survey data. The data-driven operations consist of geometrical normalisation of the amplitude response to yield exact background resistivity and attribute analysis to detect the lateral extent of 3D resistors and for anomaly-typing. Knowing the background resistivity and the type-and-lateral extents of CSEM anomalies allows a tailored 'fit-for-purpose' follow-up modelling and uncertainty appraisal of potential 3D targets. In combination with seismic and well log information, this consistent approach can yield

an unambiguous subsurface model to guide important decision making in marine exploration.

TAILORED INTERPRETATION METHOD

Geometrical normalization to determine exact background resistivity and presence of resistors at depth

For an inline marine frequency-domain CSEM survey with a dipole transmitter of length *TL* and an electric dipole receiver of length *RL* placed on the seafloor, the inline electric field at a given frequency may be transformed into geometry-normalized responses (ρ_{gnr}) which have units of resistivity, using the formula

$$\rho_{gnr} = \left(\frac{2\pi r^3}{TL.RL}\right)\frac{A}{I} \qquad (1)$$

where the quantity $K = 2\pi r^3/(TL\times RL)$ is the geometrical factor, r is the range or Tx-Rx offset in metres, *TL* and *RL* are in metres, I is the transmitter current in Amperes, and A (in volts) is the amplitude of the electric field measured by the receiver dipole. Note that the K here is equivalent to that used by Edwards (1997) to define normalised responses for time-domain marine CSEM method (i.e., $K = 2\pi r^3/(TL\times I)$). The above definition of ρ_{gnr} is thus applicable in both frequency- and time-domains. Equation (1) is analogous to the formula for defining apparent resistivity for the axial dipole-dipole configuration over a half-space in dc resistivity method applied on land (Parasnis, 1986, Appendix 8).

For illustration, in **Fig 2** are shown the amplitude and geometry-normalised responses for a half-space background 1D model of 1 Ωm (blue curves) and a canonical reservoir model consisting of a 1 Ωm background with an embedded 100m-thick layer of 50 Ωm at 1000m depth beneath a 1000 m deep sea of 0.3 Ωm resistivity. A Tx tow-height of 25m above the seafloor and a frequency of 0.1 Hz were used for this example. At short source-receiver separations, a geometry-normalized sounding curve has peak amplitude exactly equal to the average of the conductivities of seawater and the underlying seafloor (overburden) in deepwater case, but only when both the source and receivers are located on the seafloor in shallow-water case. Note the sharp peak response around 500 m Tx-Rx offset in **Fig 2b**. This first peak response is a direct measure of the seafloor resistivity. For the adopted seawater of 0.3 Ωm and seafloor of 1 Ωm resistivity, the reciprocal of the average media conductivity is 0.46 Ωm as is clearly evident in the first-peak response in **Fig 2b**. This relationship, which is exact for a seafloor Tx-Rx array, can be stated as

$$\sigma_b = 2\sigma_p - \sigma_w \qquad (2)$$

where σ_b is the local background or overburden conductivity in S/m, σ_p is the first peak response

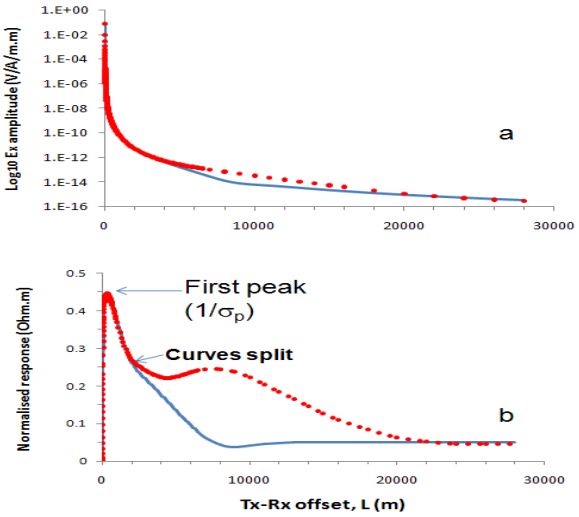

Figure 2. Comparison of single-receiver inline electric field amplitude and geometry-normalised responses. (a) MVO responses and (b) corresponding normalised responses for background model (solid blue curves) and a canonical reservoir model (red dots).

(average media conductivity) in S/m, and σ_w is the seawater conductivity in S/m. It is exact for a seafloor Tx-Rx system and provides a simple method for the direct determination of overburden resistivity using the inline dipole-dipole array especially because σ_w is always independently measured in CSEM surveys.

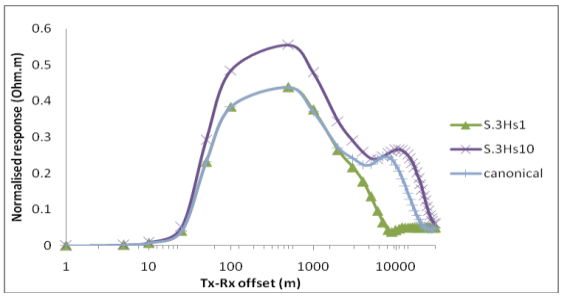

Figure 3. First peak is unique for a given seawater-overburden resistivity contrast. Seawater (S) and half-space (Hs) resistivities are indicated as well as the canonical model.

In **Fig 3**, it is demonstrated that the first-peak response is unique for a given seawater-overburden resistivity contrast such that the second-peak anomalies generated in a high-resistivity half-space cannot be confused with the signature of a thin resistor hosted in conductive sediments (i.e., the so-called canonical reservoir model). It is remarked that the sounding curve for a background half-space model and that for a laterally extensive resistor model will split at a Tx-Rx offset comparable to about twice the burial depth of the resistive horizon (e.g. see **Fig 2b**) for optimum sounding frequencies whose first-peak responses recover the exact background resistivity; this provides an initial guess of the maximum depth of occurrence of a resistive horizon. Pseudo-depth

sections of common-mid-point profiles (Sasaki & Meju, 2009), normalised by background resistivity, also offer useful clues on anomaly-type and depth locations.

3D edge-detection attributes analysis to find reservoir shape

There are different ways of finding shapes or edges of 3D objects using remotely-sensed CSEM data. He et al., (2008) use the second derivative of the magnitude versus offset curve to define the edges of a resistive reservoir. Dell'Aversana (2010) considers the symmetry properties of the in-tow and out-tow common-mid-point (CMP) sounding curves for each receiver and is favoured and extended here. The concept of detecting 3D edges through geometrical similarity analysis of in-tow and out-tow CMP sounding curves is simple: For a given receiver position, the area under the curves should be different when significant finite resistors are present in stratified media. For the ith CSEM receiver, the differences between both curves for a selected Tx-Rx offset interval $|x_1|$ to $|x_2|$, and for a given frequency, are summed to give the asymmetry measure Δ_i, as described by the space integral

$$\Delta_i = \frac{1}{b}\left(\int_{x_1}^{x_2} A_{in}\,dx - \int_{x_1}^{x_2} A_{out}\,dx\right) \qquad (3)$$

or in discrete form $\Delta_i = \frac{1}{b}\left(\sum_{x_1}^{x_2} A_{in} - \sum_{x_1}^{x_2} A_{out}\right)$,

where A_{in} and A_{out} are the respective in-tow and out-tow MVO or PVO response curves, and the local background response b can be used for site-specific normalization in the interval $|x_1|$ to $|x_2|$. The quantity Δ_i is plotted at the position of the ith CSEM receiver. The calculation is repeated for each receiver yielding lateral profiles of this edge-detection attribute for each measurement frequency. Squares of this measure are preferred for 3D map views and is termed variance attribute here **(Fig. 4)**.

In **Fig 4**, a giant 3D reservoir of x,y,z dimensions 9000m×3000m×100m and resistivity 50 Ωm is located within a homogeneous background of 1 Ωm beneath a 1800m thick seawater layer of 0.3 Ωm resistivity. The forward problem was solved using a variant of the 3D finite-difference code of Sasaki & Meju (2009). Shown are the edge-detection attributes for reservoir depths of 1000 and 1600 m below the seafloor. Notice that the reservoir's lateral limits for the different overburden thicknesses (1000 and 1600 m) are accurately sensed (Fig 4b & 4c); note that resistive sand lobes or channels can be better tracked using the new variance attribute.

Structure-constrained a priori model analysis

It is clear from the foregoing analyses (**Figs 2-4**) that reliable estimates of the parameters of a 3D target can be

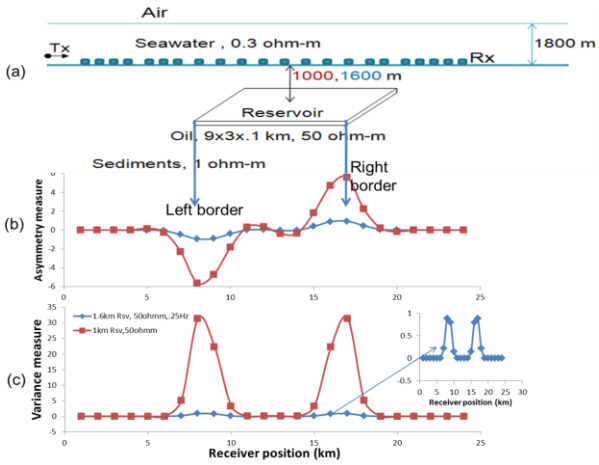

Figure 4. Test models (a) and 0.25Hz edge-detection attributes (b, asymmetry; c, variance profiles) for a line crossing the middle of a giant 3D reservoir hosted by homogeneous impermeable sediments.

obtained from geometrical analyses of sounding curves. These are used to build an initial model ($\boldsymbol{h}_{ref}$), possibly incorporating seismic or well-log constraints, and its validity tested by 3D CSEM modelling. The 3D modelling also allows the determination of any static shifts in the data (Singer et al., 2007). Only the robust features from this preliminary interpretation serve as physical constraints in the subsequent 3D inversion.

Fit-for-purpose 3D CSEM inversion

Heterogeneous overburden causes undesirable geological noise in EM field measurements (e.g. Sasaki & Meju, 2006, 2009). To improve CSEM data interpretation, we therefore account for the potentially complex overburden (and bathymetry) effects and also incorporate reliable a priori information $\boldsymbol{h}_{ref}$ in the inverse problem formulation. We minimize the function

$$U = \left\|\mathbf{W}\left[\mathbf{d}_o - f(\mathbf{m}) - Gs\right]\right\|^2 + \alpha^2\left\|\mathbf{Cm}\right\|^2 + \beta^2\left\|(D\mathbf{m} - h_{ref})\right\|^2 + \gamma^2\left\|s\right\|^2 \qquad (4)$$

and fit the observed data ($\mathbf{d}_o$) to a specified tolerance, where W is a diagonal error-weighting matrix, $f(\mathbf{m})$ is the 3D forward functional, C**m** is a smoothness measure, $\boldsymbol{h}_{ref}$ and the diagonal elements of D serve to honour the a priori information either explicitly or otherwise, while α and β are enforcement factors. Gs and γs are optional measures used to account for potential static-shifts **s** (i.e., $\mathbf{d}_o = \mathbf{d}_{undistorted} + G\mathbf{s}$) arising from small-size 3D bodies near the seabottom, which are assumed to be Gaussian. Because some important information $\boldsymbol{h}_{ref}$ have already been obtained at the pre-inversion stages, the scope of the inverse problem is drastically reduced to that of iterative refinement of only a few well parameterized target features. A 3D CSEM inversion code has been developed for this tailored approach and leans on Sasaki & Meju (2006), with the forward problem solved using the method of Sasaki & Meju (2009) but modified to take bathymetry into account. This is an important development, especially since it is then possible to

effectively interpret moderate-size CSEM field surveys on small computational platforms (Meju, 2013, in prep.).

CASE STUDY

In Figs 5-7 are shown the result of applying the above approach to CSEM data from a commercial discovery, herein called Field X for confidentiality reason.

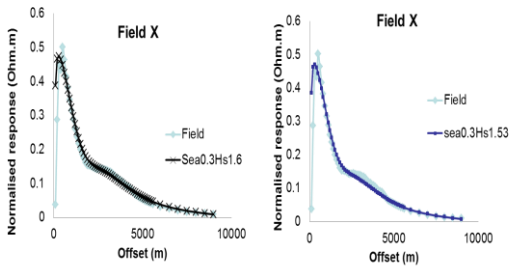

Figure 5. Example of first-peak analysis to determine overburden resistivity at Field X; black=predicted, blue=actual.

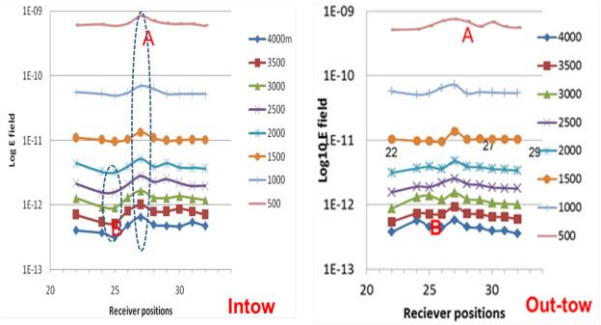

Figure 6. Pseudosections of common-depth-point amplitude profiles for an in-line CSEM survey over Field X at 0.25Hz.

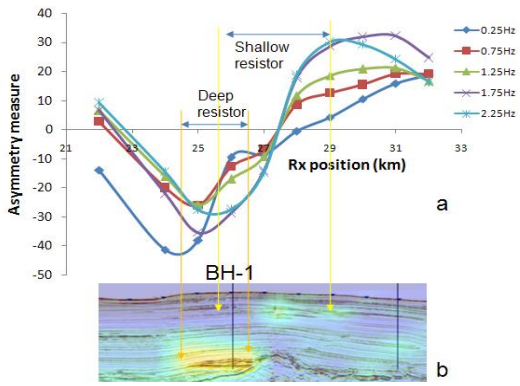

Figure 7. A comparison of multi-frequency edge-detection attribute and combined resistivity and seismic sections for a 'discovery' gas field X. The low-frequency (0.25 Hz) data locate the true edges of the deep gas reservoir while high-frequency (2.25 Hz) data locate shallow gas.

Overburden resistivity of 1.6 Ohm.m is deduced for the sounding curve shown in Fig 5, which is consistent with the resistivity well-log from the nearby site (BH-1). In Fig 6, a shallow anomaly (A) and a deeper one (B) are obvious in the common-depth-point representation of in-tow and outtow amplitudes for one survey line. The computed 3D edge-detection attributes are shown in Fig 7 and permit the localisation of anomalous 3D bodies. Subsequent 3D modelling yielded a good match to the field data after only a few iterations. Detailed results will be shown at the workshop.

DISCUSSION AND CONCLUSION

Robust 3D interpretation of CSEM surveys requires accurate estimation of heterogeneous background resistivities and lateral limits and burial depth of complex resistors. It is shown here that new geometrical CSEM attributes offer the possibility for determining exact background resistivities, lateral boundaries and depth of 3D tabular resistors. A simple approach furnishes a consistent initial structured resistivity model. Simple and inexpensive iterative modelling procedures are then used to improve the fit between the actual 3D survey data and the responses of the structured initial model, and for model appraisal. It is proposed that a reliable integration of CSEM resistivity and seismic velocity volumes can be achieved using such well-constrained CSEM inversion results, leading to potential improvement in subsurface predictions.

ACKNOWLEDGMENTS

The author thanks Murphy Oil Company and PETRONAS for permission to present the data shown here. I am grateful to Y. Sasaki for helping me understand 3D CSEM modelling. Emin Ulugergerli's assistance with 3D inversion is acknowledged.

REFERENCES

Darnet, M, M.C.K. Choo, R.-E. Plessix, M.L. Rosenquist, K. Yip-Cheong & J.W.K. Voon,2007, Detecting hydrocarbon reservoirs from CSEM data in complex settings: Application to deepwater Sabah, Malaysia, *Geophysics*, **72**, WA97-WA103.

Dell'Aversana, P., 2010, Accurate detection of resistivity anomalies using the symmetry attribute and inversion of marine CSEM data. *The Leading Edge*, **29**, 662-671.

Edwards, R. N., 1997, On the resource evaluation of marine gas hydrate deposits using sea-floor transient electric dipole-dipole methods, *Geophysics*, **62**, 63-74.

He, Z.K., K. Strack, G. Yu & Z.G. Wang, 2008. On reservoir boundary detection with marine CSEM. *Applied Geophysics*, **5**, 181-188.

Lovatini, A., E Medina, T. Campbell & K. Myers, 2010, The use of CSEM within an integrated exploration project, 72nd EAGE Conference & Exhibition, Barcelona, Spain, 14-17 June, 2010.

Parasnis, D.S., 1986, *Principles of Applied Geophysics*, Elsevier, 4th Edition.

Sasaki, Y. & M.A. Meju, 2009, Some useful characteristics of shallow and deep marine CSEM responses inferred from 3D finite-difference modelling, *Geophysics*, **74**. F67-F76. doi:10.1190/1.3168616.

Sasaki, Y. & M.A. Meju, 2006, Three-dimensional joint inversion for magnetotelluric resistivity and static shift distributions in complex media, *J. Geophys. Research*, **111**, B05101, doi:10.1029/2005JB004009.

Singer, B.S., E.B. Fainberg, P.O. Barsukov & J.K. Kjerstad, 2007, Static shift in marine electromagnetic measurements, 69th EAGE Conference & Exhibition, London UK,11-14 June, 2007. Paper D033.